JOURNAL OF THERMOPHYSICS AND HEAT TRANSFER
Vol. 33, No. 4, October–December 2019

Thermal Contact Resistance at Rough Ceramic–Metallic Joints

Mikel Garcia-Poulin* and Majid Bahrami†
Simon Fraser University, Surrey, British Columbia V3T 0A3, Canada

DOI: 10.2514/1.T5684

Engineered ceramics are widely used in a variety of industries in demanding thermal environments. In power electronics, for example, the thermal contact resistance (TCR) between ceramic insulators and metallic heat sinks can be a significant bottleneck to heat transfer. Despite this, the existing TCR literature has (for the most part) focused on metal–metal contacts. In this study, the thermal contact resistance between aluminum oxide, alumina nitride, and stainless steel is experimentally measured using the guarded heat flow meter technique, as per ASTM E1530 ("Standard Test Method for Evaluating the Resistance to Thermal Transmission of Materials by the Guarded Heat Flow Meter Technique," ASTM International STD E1530-11, West Conshohocken, PA, 2016). Tests are conducted both under vacuum and under atmospheric pressure in order to compare results with existing metal–metal TCR models. Experimental results are within a 25% rms relative difference of existing statistical-based conforming rough plastic TCR models.

Nomenclature

A_a	=	apparent contact area, m^2
A_r	=	real contact area, m^2
a	=	microcontact radius
c_1	=	hardness parameter, GPa
c_2	=	hardness parameter, GPa
E	=	bulk elasticity, GPa
F	=	contact force, N
H'	=	microhardness, GPa
H_{BR}	=	Brinell hardness, GPa
k	=	thermal conductivity, $W/(m \cdot K)$
M_g	=	molecular weight of gas
M_s	=	molecular weight of solid
m	=	average asperity slope, rad
n_s	=	number of microcontact spots
P	=	apparent contact pressure, Pa
Pr	=	Prandtl number
α_T	=	thermal accommodation coefficient
γ	=	ratio of gas specific heats
γ_p	=	Mikic plasticity index
δ	=	flatness deviation, μm
Λ	=	molecular mean free path m
λ	=	relative mean separation between planes
ν	=	Poisson ratio
σ	=	roughness, μm
σ_0	=	one unit, μm

I. Introduction

ENGINEERED ceramics are used extensively in demanding operating conditions due to their exceptional material properties. Examples include the use of aluminum nitride in electronic and power electronic packaging, which has a thermal conductivity similar to aluminum yet does not conduct electricity. Aluminum oxide is frequently used as grinding material for its hardness, as a thermal insulator in refractories due to its high melting point, and as an electrical insulator because of its high dielectric strength. In applications where thermal management is critical, such as electronics cooling, thermal resistance both within and at the interfaces of engineered ceramics can significantly influence heat transfer. The ability to model and predict heat transfer in such assemblies is critical for proper thermal design, and thus the reliability of such devices. The bulk thermal resistance of ceramics can be readily estimated by knowing its thermal conductivity using standardized tests such the ASTM STD E-1530 [1]. Spreading and constriction thermal resistances (i.e., the resistance due to cross-sectional area changes in the heat path) may be calculated using available correlations [2,3] or finite element analysis software. Thermal contact resistance (TCR), which is the resistance to heat transfer through imperfect mating surfaces, on the other hand, is more difficult to predict because it is a function of microscale surface features (e.g., surface roughness and out of flatness) as well as material surface properties (e.g., surface microhardness) that do not necessarily reflect the bulk material properties [4].

Our current knowledge of TCR is due to the work of many researchers who, for the most part, focused on metal–metal contacts [5]. In a vacuum, heat is limited to flow through the solid contact points at the interface between the surfaces because the radiation heat transfer contribution is negligible when joint temperatures are below 600°C [6]. To simplify the analysis, many studies have divided this solid resistance into micro- and macrothermal contact resistances [7]. Microresistance is caused by microscale imperfections commonly referred to as surface roughness, whereas macroresistance is caused by surface curvature, out of flatness, or macroscale periodic imperfections (waviness) [7].

Cooper, Mikic, and Yovanovich developed the famous CMY model for conforming (negligible macroimperfections) rough contacts, which assumed a Gaussian roughness distribution, equivalent joint material and surface properties, and plastic deformation of roughness peaks (asperities) [8]. Conforming rough models may be coupled with nonconforming smooth (negligible microimperfections) models to cover nonconforming rough contacts [7]. At atmospheric gas pressure, heat may pass through air gaps (both micro- and macro-) as well as through the solid contact spots; again, radiation is typically neglected. Bahrami et al. [9] and Song et al. [10] gas-gap models cover a wide range of Knudsen numbers. A more detailed review can be found in Madhusudana's book [11] and Yovanovich's review paper [5].

Metal–metal contact has dominated TCR research because metals are good thermal conductors and are the most common materials used in thermal management systems. However, ceramic TCR has not been widely studied: TCR between ceramic and metals even less so. Marotta and Fletcher studied refractory ceramic coatings on metal substrates in contact with bare aluminum [12]. Only two of the eight test cases matched Antonetti and Yovanovich's model [13] at high contact pressures, whereas none of the coatings matched Antonetti and Yovanovich's model [13] or Yip's model [14] at lower contact pressures [12]. The authors believed it might be due to the out of flatness or incorrect thermal conductivity of the coatings [12]. Chung

Received 9 December 2018; revision received 1 May 2019; accepted for publication 3 May 2019; published online 18 July 2019.

*M.S. Student, Department of Mechatronic Systems Engineering.
†Professor, Department of Mechatronic Systems Engineering; mbarahmi@sfu.ca (Corresponding Author).

et al. studied metallic coatings on aluminum oxide substrates [15]. Their aluminum and copper coatings improved thermal contact conductance by 30%. They did not compare their experimental results with any of the available models in the literature. Mirmira et al. studied interfacial contact resistance between stacks of single crystal ceramics and proposed a correlation to fit their experimental results [16].

Some experimental results did match existing metal–metal models. The experiment conducted by Aikawa and Winer on sintered silicon nitride contacts fit the modified Greenwood–Williamson contact model [17]. Similarly, Rao et al.'s experimental TCR results on Al2O3/Al-AlN metal matrix composite joints [18] were close to both Mikic's model [19] and Sridhar and Yovanovich's model [20].

The thermal resistance of joints made up of dissimilar materials is an active research topic [21]. Ceramics and metals transfer heat through different methods; metals transport heat via free electrons, whereas heat transfer in ceramics relies heavily on lattice vibrations (phonons) [21,22]. Research on thermal boundary resistance (TBR) (which is the resistance at a perfect interface between different materials due to phonon–electron, phonon–phonon, and electron–electron interactions) suggests that material pairs that differ greatly in their Debye temperatures may have a higher TBR than more similar material pairs [21,23]. This TBR is expected to be much less important than TCR due to imperfect mechanical contact [23].

Ceramics and metals are also different in their mechanical properties. From metal–metal studies, it is known that TCR is a strong function of surface microhardness (and/or elasticity), contact pressure, and surface geometry [5]. Ceramics (and aluminum oxide in particular) are an order of magnitude harder than most metals. In addition to their extreme hardness, ceramics are brittle materials, whereas metals are ductile. Under blunt indentation, ceramic deformation, although similar to metal deformation on a macroscale, is different from metals on a microscale and is characterized by brittle cone fracture above the elastic limit [24]. These cracks may initiate further microcracks at high loads [24]. Finally, ceramic surfaces can be notably different from surfaces found in typical TCR experiments, such as bead-blasted metals. Ceramics are formed from powders and sintered particles under high pressure and temperature. Depending on the grain size and sintering parameters, these materials may contain dead end surface pores.

None of the TCR models currently available in the literature have been developed based on ceramic–metal contacts or porous, fractured microcontacts. Perhaps this is because researchers have concluded that ceramic–metal contacts are not much different from metal–metal interfaces with respect to TCR. The experimental literature does not yet back up this hypothesis. Ceramic–metal contacts have only been explored in the form of coatings, and these did not match the existing models. No experimental studies have been conducted on the TCR between bulk ceramic–metal contacts (without coatings). Despite the differences in geometric, mechanical, and thermal characteristics (the triad disciplines of TCR modeling) between ceramics and metals, the existing literature (and Ref. [17] in particular) suggests that metal–metal models work well for some ceramic–ceramic contacts.

In this study, conforming rough TCR between stainless-steel 304 (SS304) and aluminum oxide and aluminum nitride is measured using a guarded heat flow meter technique, as per ASTM STD E1530 [1]. Our experimental results are then compared with available statistical TCR metal–metal models and show that metal–metal models are in reasonable agreement with ceramic–metal joints.

II. Statistical TCR Model Implementation

The statistical TCR models used in this work all assume that one surface is rough and the other is perfectly smooth (see Fig. 1 [25]). The rough surface takes on the effective surface properties of both real surfaces. These properties are calculated with Eqs. (1–3), whereas Eq. (4) is exclusively used for models that assume elastic deformation. Plastic models assume that the microhardness of the effective rough surface is equal to the microhardness of the softer material. Microhardness, and not bulk hardness, is recommended for plastic TCR models [4]:

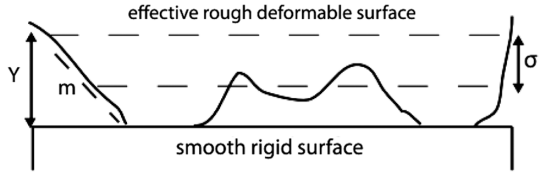

Fig. 1 Equivalent rough surface of conforming rough Gaussian contacts [25].

$$\sigma = \sqrt{\sigma_{\text{metal}}^2 + \sigma_{\text{ceramic}}^2} \tag{1}$$

$$m = \sqrt{m_{\text{metal}}^2 + m_{\text{ceramic}}^2} \tag{2}$$

$$k = \frac{2k_{\text{metal}}k_{\text{ceramic}}}{(k_{\text{metal}} + k_{\text{ceramic}})} \tag{3}$$

$$E = \left(\frac{1-\nu_{\text{ceramic}}^2}{E_{\text{ceramic}}} + \frac{1-\nu_{\text{metal}}^2}{E_{\text{metal}}}\right)^{-1} \tag{4}$$

The CMY model with plastic deformation [26], the CMY model with elastic deformation [19], and Bahrami et al.'s scale analysis model [27] were selected for comparison with the present experimental results. The scale analysis model does not differ significantly from the CMY plastic model [27]. Both are used in this work because the scale analysis model, although easy to implement, has a scaling factor that was derived based on metal–metal TCR experiments. The appropriateness of this scaling factor for ceramic–metal joints is not known a priori. The CMY and the scale analysis models' equations are listed in Table 1 for the reader's convenience [26,27,28]. Implementation of the CMY model requires iteration on the microhardness and mean plane separation [from Eqs. (5–11), excluding Eq. (7)] between the two effective surfaces. The bulk material hardness is used as an initial guess for this iteration, which is completed when the microhardness recalculations are negligibly different. Equations (12–16) complete the CMY model for conforming rough contact. Correlations that simplify the CMY model implementation are available in the literature [5] but are not used in this work.

Table 1 Summary of thermal contact resistance CMY model

Equation no.	Equation	Reference
(5)	$c_1 = 7.339e^{(-0.001695)(T-25.2)}$	[26]
(6)	$c_2 = -0.279$	[26]
(7)	$\lambda_{\text{elastic}} = \sqrt{2}\text{erfc}^{-1}\left(\frac{4\sqrt{2}P}{mE}\right)$	[26]
(8)	$\lambda_{\text{plastic}} = \sqrt{2}\text{erfc}^{-1}\left(\frac{2P}{H'}\right)$	[26]
(9)	$a = \text{erfc}\left(\frac{\lambda}{\sqrt{2}}\right)\frac{\sigma}{m}e^{\frac{\lambda^2}{2}}\sqrt{\frac{8}{\pi}}$	[26]
(10)	$D_V = a\sqrt{2\pi}$	[26]
(11)	$H' = c_1\left(\frac{DV}{10^{-6}}\right)^{c_2}$	[26]
(12)	$\frac{A_{\text{real}}}{A_{\text{apparent}}} = \frac{1}{2}\text{erfc}\left(\frac{\lambda}{\sqrt{2}}\right)$	[26]
(13)	$n = \frac{(1/16)(m/\sigma)^2 e^{-\lambda^2}}{\text{erfc}\left(\frac{\lambda}{\sqrt{2}}\right)}$	[26]
(14)	$\psi = (1 - \sqrt{\frac{A_{\text{real}}}{A_{\text{apparent}}}})^{1.5}$	[26]
(15)	$h_{\text{solid}} = \frac{2nak}{\psi}$	[26]
(16)	$\text{TCR}_{\text{solid}} = \frac{1}{h_{\text{solid}}A_{\text{apparent}}}$	[26]
(17)	$K = \frac{H_B}{H_{\text{BGM}}}$	[27,28]
(18)	$c_1 = H_{\text{BGM}}(4 - 5.77K + 4K^2 - 0.61K^3)$	[27,28]
(19)	$c_2 = -0.57 + 0.82K - 0.41K^2 + 0.06K^3$	[27,28]
(20)	$H' = c_1\left(\frac{\sigma}{m\sigma_0}\right)^{c_2}$	[27]
(21)	$\text{TCR}_{\text{solid}} = \frac{0.565\ H'\left(\frac{\sigma}{m}\right)}{k_s F}$	[27]

Table 2 Gas-gap equations

Equation no.	Equation	Reference
(22)	$\Lambda = \Lambda_0\left(\frac{P_0}{P_g}\right)\left(\frac{T_g}{T_0}\right)$	[9]
(23)	For diatomic or polyatomic gases, $M_g^* = 1.4M_g$	[9]
(24)	$\mu = \frac{M_g}{M_s}$	[9]
(25)	$\alpha_T = e^{-0.57\left(\frac{T_s-T_0}{T_0}\right)}\left(\frac{M_g^*}{6.8+M_g^*}\right) + \left(\frac{2.4\mu}{(1+\mu)^2}\right)\left(1-e^{-0.57\left(\frac{T_s-T_0}{T_0}\right)}\right)$	[9]
(26)	$M = \left(\frac{2-\alpha_{T1}}{\alpha_{T1}} + \frac{2-\alpha_{T2}}{\alpha_{T2}}\right)\left(\frac{2\gamma}{1+\gamma}\right)\left(\frac{\Lambda}{Pr}\right)$	[9]
(27)	When $0.01 \le \frac{M}{\sigma} \le 1$, $f_g = 1.063 + 0.0471(4-\lambda)^{1.68}(\ell_n(\frac{\sigma}{M}))^{0.84}$	[26,30]
(28)	When $\frac{M}{\sigma} \ge 1$, $f_g = 1 + 0.06(\frac{\sigma}{M})^{0.8}$	[26,30]
(29)	$\mathrm{TCR}_{\mathrm{gas}} = \frac{1}{k_g A_a f_g}(M + \sigma\lambda)$	[26]
(30)	$\mathrm{TCR}_{\mathrm{gas-simplified}} = \frac{1}{k_g A_a}(M + \sigma\lambda)$	[9]
(31)	$\mathrm{TCR}_j = \left(\frac{1}{\mathrm{TCR}_{\mathrm{solid}}} + \frac{1}{\mathrm{TCR}_{\mathrm{gas}}}\right)^{-1}$	[9]

Microhardness is calculated only for the stainless-steel surfaces because the ceramic surfaces have expected microhardness [29] in excess of three times that of stainless steel; thus, the effective joint microhardness is the stainless-steel microhardness. Several correlations for microhardness coefficients (c1 and c2) used for the microhardness of stainless steel are available in the literature, and two different ones [Eqs. (5), (6), and (17–19)] are selected for our implementation of the CMY and scale analysis models. Equations (20) and (21) complete the scale analysis model for conforming rough contact. The CMY elastic model may be calculated from Eqs. (7) and (9) to Eq. (16), excluding Eq. (11). Equations (16) and (21) represent the microthermal resistance due to imperfect contact at the conforming surfaces, which is caused by surface roughness of the mating surfaces. Under atmospheric gas pressure, TCR calculations require an additional model to calculate the resistance of the gas gaps in between the contacting surfaces. Two of these models are tabulated in Table 2, with one being a simplification [Eqs. (22–26) and (30)] [9] of the other [(Eqs. (22–29)] [26,30,31]. Both models yield close results for the present tests. The simplified model of Bahrami et al. [9] neglects the roughness of the real contact area (order of 2% for bare metal–metal contact) and assumes that the gas gaps may be approximated by two parallel plates with the apparent contact area held a distance equal to the mean plane separation apart from each other. In this work, the simplified model is used with the scale analysis model and the full gas-gap model with integral approximation is used with the CMY models so that both a detailed model and a simpler model are compared with the results. Because the heat is limited to transfer either through the solid contact points or through the gas, the gas resistance and the solid resistance are in parallel, as seen in Eq. (31).

III. Experimental Setup

Thermal conductivities of the stainless-steel 304 (2 and 4 mm thick) and 99.5% aluminum oxide (2 mm thick) samples were measured per ASTM STD E1530 using a guarded heat flow meter setup available at our laboratory [1] (see Fig. 2). ARMCO iron heat flux meters with a diameter of 25.4 mm (1 in.) were used with six thermocouples located at the center of the flux meters 5 mm apart from each other and 10 mm apart from the edges. Aluminum nitride thermal conductivity was not measured because the combination of small sample thickness (0.4 mm) and high expected thermal conductivity [170 $\mathrm{W/(m \cdot K)}$] results in a negligible deviation in thermal resistance (0.002 K/W) with a reasonable difference (30%) in expected and actual thermal conductivities. To measure the TCR between ceramic and metallic surfaces, the same guarded heat flow meter setup was used. The heat flow through the joint was measured per ASTM STD E1530 using the cylindrical ARMCO iron heat flux meters. To measure the temperature difference across the metal–ceramic–metal joint thermocouples (Omega, T type, ±1°C) were inserted into each metal sample. All measurements were conducted with a single ceramic (or metal) sample in between two metal samples equipped with thermocouples. Thermocouples that exhibited minimal temperature (less than 0.3°C) difference in a hot water bath (from ambient to 100°C) were selected for insertion into the metal samples

To prepare the metal samples for the TCR experiment, stainless-steel 304 disks were first turned on a lathe, lapped (to ensure conforming contact) off site, and then bead blasted at an in-house machine shop to create random (Gaussian) roughness. Measured surface roughness values are provided in Table 3.

All sample roughness and approximate flatness measurements (less than 0.5μm across sample diameter) were measured by profilometer (skidless diamond tip, Mitutoyo Surftest SJ-400; flatness resolution of 0.3 μm over 25 mm) in our laboratory. Polished and as-fired aluminum oxide and polished aluminum nitride 25.4-mm-diameter (1-in.-diameter) disks were ordered from Ortech Advanced Ceramics and Stellar Ceramics, respectively.

TCR measurements were conducted both in a vacuum and under atmospheric gas pressure. First a rotary pump and then a diffusion pump were used to create a high vacuum. During measurement, vacuum pressure was maintained between 1.25 and 4 mPa ($4 \cdot 10^{-5}$ mbar or $3 \cdot 10^{-5}$ torr) and was measured with a Penning gauge. Thermal measurements were taken at steady-state conditions determined to be when the total thermal resistance between the heat flux meters changed less than 0.12% for over 30 min and 0.06% over 10 min. On average, tests exceeded 3 h. Details of the uncertainty analysis are provided in the Appendix. Lateral heat losses off the test column are neglected in vacuum because temperature differences are low. In atmospheric pressure, lateral heat losses are also neglected because it is assumed there will be no convection within the glass bell chamber enclosing the experimental test column. Air within the chamber insulates the test column. Thermal conductivity tests of the sample material were not significantly different with and without insulation. Heat losses are temperature dependent but do not exceed 3% of average heat through the joint.

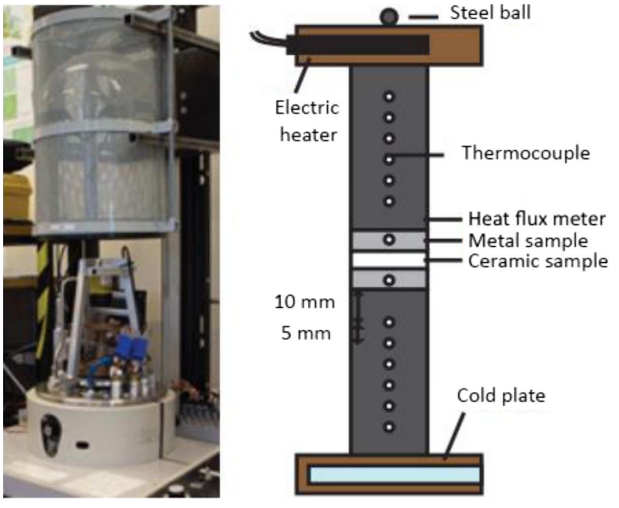

Fig. 2 Guarded heat flow meter experimental setup.

Table 3 Bulk material properties

	Thermal conductivity, W/(m · K)	Approx. microhardness, GPa	Bulk elasticity, GPa	Poisson ratio
AlN	170	10	300	0.24
Al2O3	25.2	15	300	0.21
SS304	16.8	3.4	200	0.29

Table 4 Surface properties

Properties	Measured rms roughness, μm	Calculated asperity slope, rad	Approximate calculated microhardness, GPa
Polished AlN	0.03	0.0092	10
Polished Al2O3	0.28	0.048	15
As-fired Al2O3	1.1	0.13	15
Lapped SS304	0.33	0.043	3.85
Bead-blasted SS304 control	2.8	0.13	2.9
Bead-blasted SS304 test	1.9	0.11	3.1

Table 5 Experimental joints

Joint number	Metal sample	Ceramic sample
1	Lapped SS304	Bead-blasted SS304 control
2	Bead-blasted SS304 test	Polished Al2O3
3	Bead-blasted SS304 test	Polished AlN
4	Lapped SS304	Polished Al2O3
5	Lapped SS304	Polished AlN
6	Lapped SS304	As-fired A l2O3
7	Bead-blasted SS304 test	As-fired Al2O3

Bulk material properties are tabulated in Table 3. Surface properties are listed in Table 4. Thermal conductivity and roughness were measured in the laboratory, as previously described. Approximate microhardness, bulk elasticity, and Poisson ratio values were taken from the literature. Table 5 lists the experimental joints used in the experiment.

IV. Experimental Results

Thermal conductivity measurements of the stainless steel and aluminum oxide are presented in Fig. 3. The linear curve fits (y intercept $= 32.87$ and slope $= -0.08526$ for alumina, and y intercept $= 13.70$ and slope $= 0.03407$ for stainless steel) in Fig. 3 were used to deconvolute the TCR from all the experimental results in this work.

To investigate the repeatability of the results, the TCR of a metal–ceramic–metal joint (joint 2) was mounted and measured five times

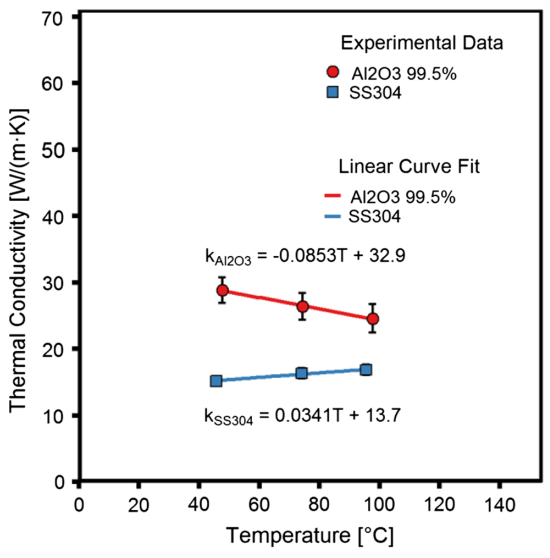

Fig. 3 Thermal conductivity of alumina and stainless steel.

(rotating sample and remounting each time) under atmospheric pressure. As seen in Fig. 4b, remounting the joint did not result in a significant difference in TCR in atmospheric pressure. Similarly, Fig. 4a illustrates the same test but done under high vacuum pressure (joint 4).

The deviations in the results are insignificant at high contact pressure but become significant and are outside the expected uncertainty at low contact pressures. The authors expect that this is reasonable, considering that the sample was rotated and remounted in between each run, and a high random error is only present at low contact pressures, especially where TCR is most sensitive to initial contact area and hysteresis. To provide a benchmark for comparison with all of the ceramic–metal tests, the TCR between lapped stainless steel and bead-blasted stainless steel was measured both in vacuum and under atmospheric pressure. The experimental results under vacuum are presented in Fig. 5a, and those in atmospheric pressure are in Fig. 5b along with the TCR models for conforming the rough contact previously described. As the results show, the experimental data match both plastic models under vacuum (14% rms relative difference) and atmospheric pressure (18% rms relative difference). It is clear from Fig. 5a that the plastic deformation assumption of the asperities predicts the data more accurately for these contact pressures. Lambert and Fletcher's correlation for the asperity slope as a function of surface roughness [Eq. (32)] [32] is used for the stainless-steel surfaces in this study. This is done with confidence, despite the high error associated with asperity correlations, because the TCR data are in good agreement with the model in Figs. 6 and 7. Use of the measured asperity slope in the model did not adequately capture the steel–steel experimental TCR. The cause for this is unknown but may be due to a poor asperity slope measurement due to limitations of the profilometer tip or use of a different bead-blasting technique from previous studies:

$$m_{SS304} = 0.076(\sigma)^{0.52} \tag{32}$$

V. Rough Metals and Smooth Ceramics

TCR results between polished ceramics and bead-blasted stainless steel under high vacuum are presented in Fig. 6a. The same models using the material and surface properties of both the ceramic and the stainless steel are also shown. They are in good agreement with the data (joint 2: 14% rms error; and joint 3: 13% rms relative difference). Again, based on Fig. 6a, the deformation of the asperities is assumed to be plastic. This is as expected because the stainless steel is the rough surface, and therefore it is the stainless steel's asperities that are deforming on the smoother ceramic. This is consistent with Mikic's plasticity index, shown in Eq. (33), which indicates plastic asperity deformation when less than or equal to 0.33 and elastic asperity deformation when greater than or equal to 3.0 [19]. Joint 1 (SS304 and SS304) has a Mikic plasticity index of 0.19, joint 2 has a Mikic plasticity index of 0.21, and joint 3 has one of 0.22:

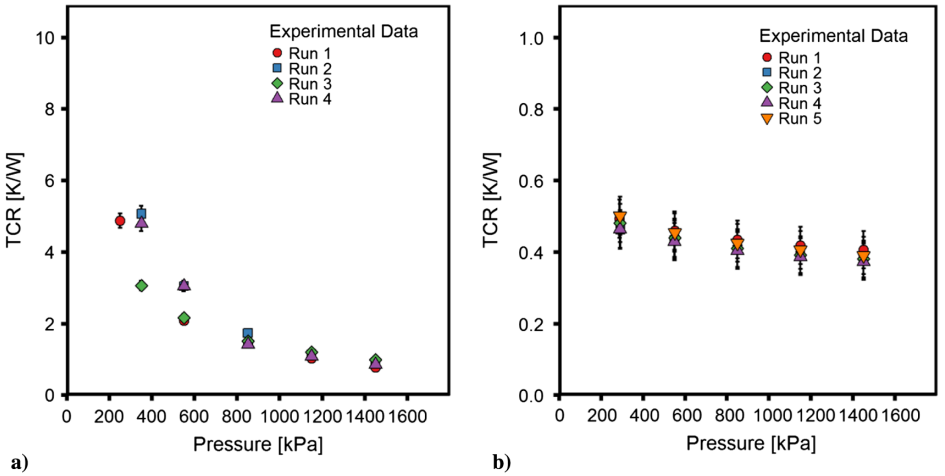

Fig. 4 Repeatability of TCR experiment in a) high vacuum pressure (joint 4) and b) atmospheric pressure (joint 2).

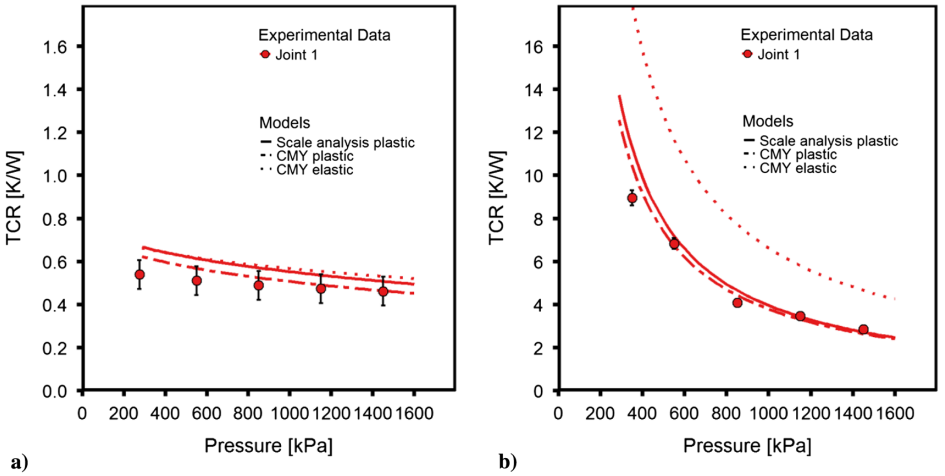

Fig. 5 TCR between lapped stainless steel and bead-blasted stainless steel in a) high vacuum and b) atmospheric pressure.

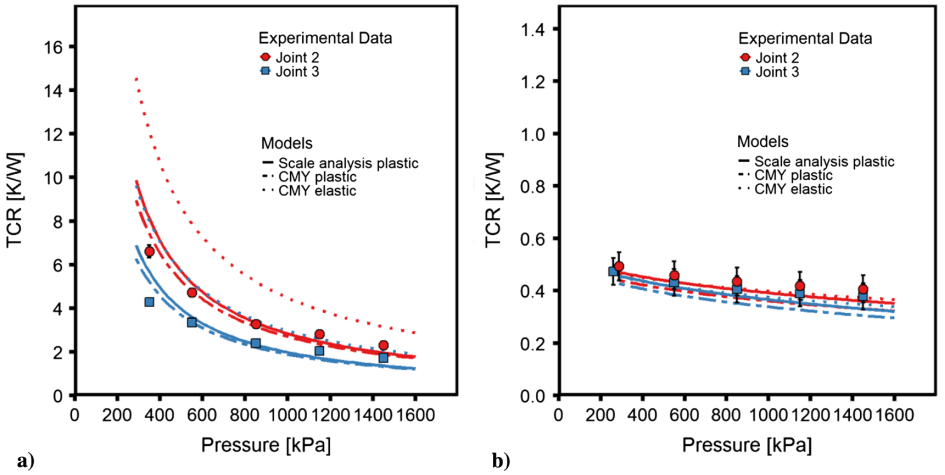

Fig. 6 TCR between bead-blasted stainless steel and polished ceramics in a) high vacuum and b) atmospheric pressure.

$$\gamma_p = \frac{H'}{Em} \tag{33}$$

In Fig. 6b, the TCR between these same samples is shown under atmospheric pressure. All the models fit the data within the uncertainty of the measurements (joint 2: 7.9% rms relative difference; and joint 3: 7.7% rms relative difference). Under atmospheric pressure, the elastic models are not significantly different from the plastic models because the presence of the air in the joint reduces the sensitivity of the model to the deformation of asperities. In addition, the TCR is reduced by an order of magnitude with a gas in the joint, which is similar to metal–metal contact.

The correlation used for the average asperity slope of the ceramic is not influential on the result because the ceramic is much smoother than the stainless steel. It holds, then, that the stainless steel's asperity

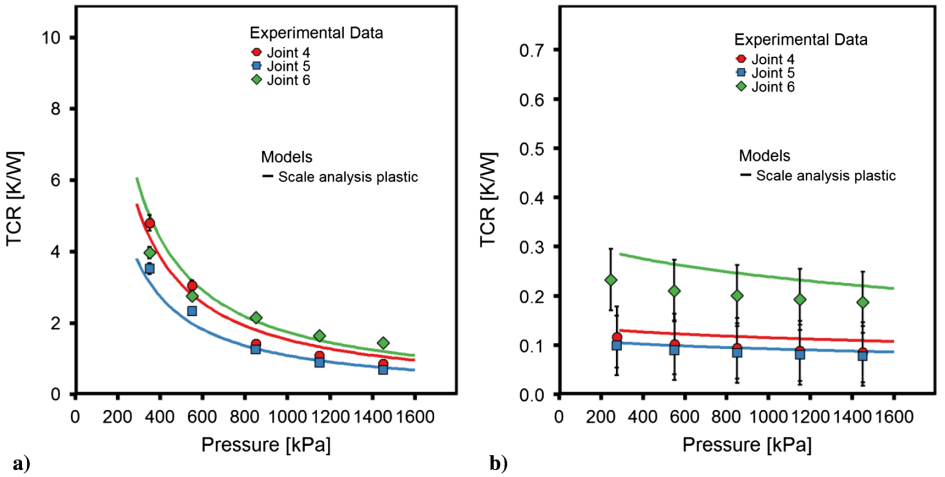

Fig. 7 TCR between ceramics and lapped stainless steel in a) high vacuum and b) atmospheric pressure.

correlation is more influential on the models' results because its roughness determines the effective roughness and effective asperity slope in the model.

Due to the similarity between the metal–metal models and ceramic–metal data, the authors conclude that the plastic conforming rough contact metal–metal models are appropriate for ceramic–metal joints when the metal is relatively rough and the ceramic is relatively smooth. In addition, the elastic CMY model is also appropriate in atmospheric pressure only. Because the deformation of the asperities is plastic and both plastic models yield similar results for ceramic stainless-steel contacts, further figures contain the scale analysis model only for simplicity.

VI. Smooth Metals and Rough Ceramics

If the ceramic is rough and the metal is smooth, then it is expected that the metal sample will deform under the harder ceramic asperities. However, the metal–metal TCR models do not consider this because they assume that the effective rough sample is the softer material and the perfectly smooth sample is the material that experiences no deformation. To test if these models work despite this assumption, rough and smooth ceramics (polished and as fired) were put into contact with smooth metals (lapped). Figures 7a and 7b show the results of this experiment in a high vacuum and atmospheric pressure. In both cases, the models are in reasonable agreement with the experimental data (joint 4: 20% rms relative difference in vacuum and 24% rms relative difference in atmospheric pressure; joint 5: 9.9% rms relative difference in vacuum and 11% rms relative difference in atmospheric pressure; and joint 6: 16% rms relative difference in vacuum and 22% rms relative difference in atmospheric pressure), which strongly suggest that the metal–metal models are appropriate for ceramic–metal joints, despite the deformation assumption. Antonetti et al.'s correlation [33] [Eq. (34)] for the asperity slope as a function of roughness was selected for the ceramic surfaces because Lambert and Fletcher's correlation [32] resulted in a larger difference from the model and experimental data. It is reasonable that one correlation is appropriate for ceramics and less so for the bead-blasted metals in this experiment because the surfaces are, in truth, formed by completely different processes. Again, for smooth metals with rough ceramics, the correlation used on the stainless steel is not influential:

$$m_{\text{ceramic}} = 0.124(\sigma)^{0.743} \tag{34}$$

VII. Rough Metals and Rough Ceramics

Finally, using Eq. (32) for the asperity slope of the bead-blasted stainless steel and Eq. (34) for the asperity slope of the as-fired aluminum oxide, the theoretical TCR for conforming rough stainless steel and conforming rough ceramic is compared with experimental data in Fig. 8a in vacuum and Fig. 8b in atmospheric pressure. In both cases, the scale analysis model captures the trend of the data and is in reasonable agreement (18% rms relative difference in vacuum and 14% rms relative difference in atmospheric pressure).

VIII. Conclusions

Experimental thermal contact resistance (TCR) results between conforming rough stainless steel and aluminum oxide and aluminum nitride contacts were presented. The results adequately agreed with the available statistical metal–metal TCR models with the use of

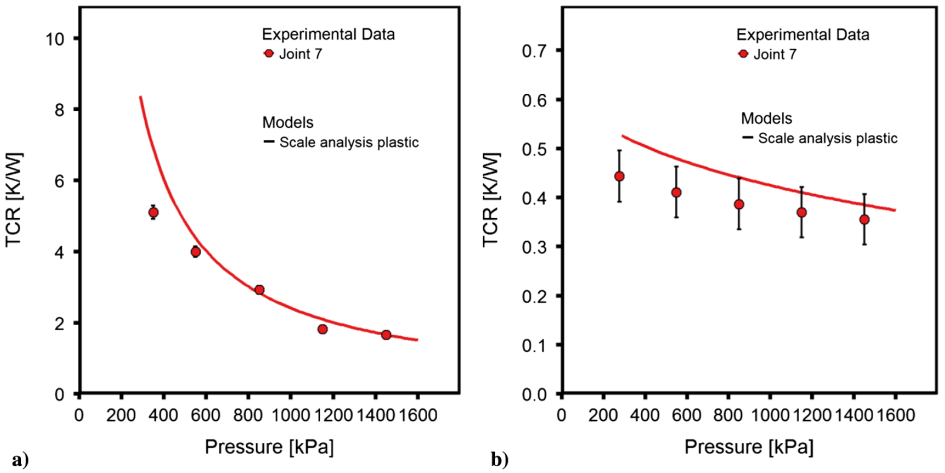

Fig. 8 TCR between as-fired alumina and bead-blasted stainless steel in a) high vacuum and b) atmospheric pressure.

certain asperity slope estimations. This strongly indicated that metal–metal TCR models were perfectly suitable for estimating ceramic–metal TCR despite the differences in material manufacture, surface features (porosity), microscale deformation characteristics, and thermal conduction.

RMS relative difference between the plastic models and the data did not exceed 21% in vacuum or 24% in atmospheric pressure. The average rms relative differences for the scale analysis model were 15 and 12% for the plastic CMY model. Most large deviations of the experimental data from the plastic models were observed at low contact pressures, which were consistent with metal–metal contacts.

Appendix: Uncertainty Calculation

The experimental data were analyzed in the *R* programming language. All linear curve fits were performed with *R*. The following equations were used in the uncertainty analysis:

$$u\mathrm{Rel}_{Q_{1\text{ or }2}} = \sqrt{\frac{u\mathrm{Abs}^2_{k_{\mathrm{HFM}}}}{k^2_{\mathrm{HFM}}} + \frac{u\mathrm{Abs}^2_{A}}{A^2} + \frac{u\mathrm{Abs}^2_{(\mathrm{d}T/\mathrm{d}x)}}{(\mathrm{d}T/\mathrm{d}x)^2}}$$

$$u\mathrm{Rel}_{Q_{\mathrm{avg}}} = \sqrt{u\mathrm{Abs}^2_{Q1} + u\mathrm{Abs}^2_{Q2}}$$

$$u\mathrm{Rel}^2_{(Qt/kA)} = \sqrt{\frac{u\mathrm{Abs}^2_{A}}{A^2} + \frac{u\mathrm{Abs}^2_{t}}{t^2} + \frac{u\mathrm{Abs}^2_{k}}{k^2} + ul\mathrm{Rel}^2_{Q_{\mathrm{avg}}}}$$

$$u\mathrm{Abs}_{T_{\mathrm{int1\text{ or }2}}} = \sqrt{u\mathrm{Abs}^2_{(Qt/kA)} + u\mathrm{Abs}^2_{\mathrm{TC}}}$$

$$u\mathrm{Abs}_{dT} = \sqrt{u\mathrm{Abs}^2_{T\mathrm{int}_1} + u\mathrm{Abs}^2_{T\mathrm{int}_1}}$$

$$u\mathrm{Rel}_{R_j} = \sqrt{u\mathrm{Rel}^2_{dT} + u\mathrm{Rel}^2_{Q_{\mathrm{avg}}}}$$

$$u\mathrm{Rel}_{R\mathrm{met\text{ or }cer}} = \sqrt{\frac{u\mathrm{Abs}^2_{A}}{A^2} + \frac{u\mathrm{Abs}^2_{t}}{t^2} + \frac{u\mathrm{Abs}^2_{k}}{k^2}}$$

$$u\mathrm{Abs}_{2\mathrm{TCR}} = \sqrt{u\mathrm{Abs}^2_{R_j} + u\mathrm{Abs}^2_{R_{\mathrm{cer}}} + u\mathrm{Abs}_{R_{\mathrm{met}}}}$$

$$u\mathrm{Rel}_{\mathrm{TCR}} = \frac{u\mathrm{Abs}_{\mathrm{TCR}}}{2\mathrm{TCR}}$$

Acknowledgments

The authors would like to express their gratitude to Delta-Q Technologies Corporation and the National Sciences and Engineering Research Council of Canada (NSERC) for funding this research under NSERC Collaborative Research Development (CRD) grant PJ488777. The authors would like to thank Chris Botting and Eric Lau of Delta-Q Technologies for their advice and many discussions, the team at Simon Fraser University's (SFU's) Faculty of Science Machine Shop for help preparing the stainless-steel samples, and Wendell Huttema for his help with the vacuum setup at Laboratory for Alternative Energy Conversion (LAEC). Finally, a big thank you to the team at SFU's 4D Labs for access to their facilities.

References

[1] "Standard Test Method for Evaluating the Resistance to Thermal Transmission of Materials by the Guarded Heat Flow Meter Technique," ASTM International STD E1530-11, West Conshohocken, PA, 2016. doi:10.1520/E1530-11R16

[2] Gholami, A., and Bahrami, M., "Thermal Spreading Resistance Inside Anisotropic Plates with Arbitrarily Located Hotspots," *Journal of Thermophysics and Heat Transfer*, Vol. 28, No. 4, 2014, pp. 679–686. doi:10.2514/1.T4428

[3] Razavi, M., Muzychka, Y. S., and Kocabiyik, S., "Review of Advances in Thermal Spreading Resistance Problems," *Journal of Thermophysics and Heat Transfer*, Vol. 30, No. 4, 2016, pp. 863–879. doi:10.2514/1.T4801

[4] Hegazy, A. A.-H., "Thermal Joint Conductance of Conforming Rough Surfaces: Effect of Surface Micro-Hardness Variation," Ph.D. Thesis, Univ. of Waterloo, Waterloo, ON, Canada, 1985.

[5] Yovanovich, M. M., "Four Decades of Research on Thermal Contact, Gap, and Joint Resistance in Microelectronics," *IEEE Transactions on Components and Packaging Technologies*, Vol. 28, No. 2, 2005, pp. 182–206. doi:10.1109/TCAPT.2005.848483

[6] Bejan, A., and Kraus, A. D., *Heat Transfer Handbook*, Wiley, New York, 2003.

[7] Bahrami, M., Culham, J. R., Yovanovich, M. M., and Schneider, G. E., "Thermal Contact Resistance of Nonconforming Rough Surfaces, Part 1: Contact Mechanics Model," *Journal of Thermophysics and Heat Transfer*, Vol. 18, No. 2, 2004, pp. 209–217. doi:10.2514/1.2661

[8] Cooper, M. G., Mikic, B. B., and Yovanovich, M. M., "Thermal Contact Conductance," *International Journal of Heat and Mass Transfer*, Vol. 12, No. 3, 1969, pp. 279–300. doi:10.1016/0017-9310(69)90011-8

[9] Bahrami, M., Yovanovich, M. M., and Culham, J. R., "Thermal Joint Resistances of Conforming Rough Surfaces with Gas-Filled Gaps," *Journal of Thermophysics and Heat Transfer*, Vol. 18, No. 3, 2004, pp. 318–325. doi:10.2514/1.5480

[10] Song, S., Yovanovich, M. M., and Goodman, F. O., "Thermal Gap Conductance of Conforming Surfaces in Contact," *Journal of Heat Transfer*, Vol. 115, No. 3, 1993, pp. 533–540. doi:10.1115/1.2910719

[11] Madhusudana, C. V., *Thermal Contact Conductance*, 2nd ed., Springer, Sydney, 2014. doi:10.1007/978-3-319-01276-6

[12] Marotta, E., and Fletcher, L. S., "Thermal Contact Conductance of Refractory Ceramic Coatings," *Journal of Thermophysics and Heat Transfer*, Vol. 10, No. 1, 1996, pp. 10–18. doi:10.2514/3.746

[13] Antonetti, V. W., and Yovanovich, M. M., "Enhancement of Thermal Contact Conductance by Metallic Coatings: Theory and Experiment," *Journal of Heat Transfer*, Vol. 107, No. 3, 1985, pp. 513–519. doi:10.1115/1.3247454

[14] Yip, F., "The Effect of Oxide Films on Thermal Contact Resistance," *Thermophysics and Heat Transfer Conference*, AIAA Paper 1974-0693, 1974. doi:10.2514/6.1974-693

[15] Chung, K. C., Benson, H. K., and Sheffield, J. W., "Thermal Contact Conductance of Ceramic Substrate Junctions," *Journal of Heat Transfer*, Vol. 117, No. 2, 1995, pp. 508–510. doi:10.1115/1.2822552

[16] Mirmira, S. R., Fletcher, L. S., and Baker, K. W., "Interfacial Contact Resistance of Single-Crystal Ceramics for Solar Concentrators," *Journal of Thermophysics and Heat Transfer*, Vol. 13, No. 1, 1999, pp. 110–116. doi:10.2514/2.6407

[17] Aikawa, T., and Winer, W. O., "Thermal Contact Conductance Across Si3N4—Si3N4 Contact," *Wear*, Vol. 177, No. 1, 1994, pp. 25–32. doi:10.1016/0043-1648(94)90114-7

[18] Rao, V. V., Krishna Murthy, M. V., and Nagaraju, J., "Thermal Conductivity and Thermal Contact Conductance Studies on Al2O3/Al-AlN Metal Matrix Composite," *Composites Science and Technology*, Vol. 64, No. 16, 2004, pp. 2459–2462. doi:10.1016/j.compscitech.2004.05.009

[19] Mikic, B. B., "Thermal Contact Conductance; Theoretical Considerations," *International Journal of Heat and Mass Transfer*, Vol. 17, No. 2, 1974, pp. 205–214. doi:10.1016/0017-9310(74)90082-9

[20] Sridhar, M. R., and Yovanovich, M. M., "Elastoplastic Contact Conductance Model for Isotropic Conforming Rough Surfaces and Comparison with Experiments," *Journal of Heat Transfer*, Vol. 118, No. 1, 1996, pp. 3–9. doi:10.1115/1.2824065

[21] Li, M., Wang, Y., Zhou, J., Ren, J., and Li, B., "Thermal Boundary Conductance Across Metal-Nonmetal Interfaces: Effects of Electron-Phonon Coupling Both in Metal and at Interface," *European Physical Journal B*, Vol. 88, No. 6, 2015, pp. 1–7. doi:10.1140/epjb/e2015-50771-8

[22] Majumdar, A., and Reddy, P., "Role of Electron-Phonon Coupling in Thermal Conductance of Metal-Nonmetal Interfaces," *Applied Physics Letters*, Vol. 84, No. 23, 2004, pp. 4768–4770. doi:10.1063/1.1758301

[23] Swartz, E. T., and Pohl, R. O., "Thermal Boundary Resistance," *Reviews of Modern Physics*, Vol. 61, No. 3, 1989, pp. 605–668. doi:10.1103/RevModPhys.61.605

[24] Lawn, B. R., "Indentation of Ceramics with Spheres: A Century After Hertz," *Journal of the American Ceramic Society*, Vol. 81, No. 8, 1998, pp. 1977–1994.
doi:10.1111/(ISSN)1551-2916

[25] Bahrami, M., Culham, J. R., and Yovanovich, M. M., "Thermal Resistances of Gaseous Gap for Conforming Rough Contacts," *42nd AIAA Aerospace Sciences Meeting and Exhibit*, AIAA Paper 2004-0821, 2004.
doi:10.2514/6.2004-821

[26] Yovanovich, M. M., "Micro and Macro Hardness Measurements, Correlations, and Contact Models," *44th AIAA Aerospace Sciences Meeting and Exhibit*, AIAA Paper 2006-0979, 2006.
doi:10.2514/6.2006-979

[27] Bahrami, M., Culham, J. R., and Yovanovich, M. M., "Modeling Thermal Contact Resistance: A Scale Analysis Approach," *Journal of Heat Transfer*, Vol. 126, No. 6, 2004, pp. 896–905.
doi:10.1115/1.1795238

[28] Sridhar, M. R., and Yovanovich, M. M., "Empirical Methods to Predict Vickers Microhardness," *Wear*, Vol. 193, No. 1, 1996, pp. 91–98.
doi:10.1016/0043-1648(95)06681-0

[29] Auerkari, P., "Mechanical and Physical Properties of Engineering Alumina Ceramics," VTT Manufacturing Technology, Espoo, Finland, 1996.

[30] Negus, K. J., and Yovanovich, M. M., "Correlation of the Gap Conductance Integral for Conforming Rough Surfaces," *Journal of Thermophysics and Heat Transfer*, Vol. 2, No. 3, 1988, pp. 279–281.
doi:10.2514/3.56224

[31] Yovanovich, M. M., DeVaal, J., and Hegazy, A., "A Statistical Model to Predict Thermal Gap Conductance Between Conforming Rough Surfaces," *3rd Joint Thermophysics, Fluids, Plasma and Heat Transfer Conference*, AIAA Paper 1982-0888, 1982.
doi:10.2514/6.1982-888

[32] Lambert, M. A., and Fletcher, L. S., "Thermal Contact Conductance of Spherical Rough Metals," *Journal of Heat Transfer*, Vol. 119, No. 4, 1997, pp. 684–690.
doi:10.1115/1.2824172

[33] Antonetti, V. W., Whittle, T. D., and Simons, R. E., "An Approximate Thermal Contact Conductance Correlation," *Journal of Electronic Packaging*, Vol. 115, No. 1, 1993, pp. 131–134.
doi:10.1115/1.2909293